# Core−Shell Structures of Silica−Organic Pigment Nanohybrids Visualized by Electron Spectroscopic Imaging

**Shin Horiuchi,[†] Shinji Horie,[‡] and Kunihiro Ichimura*[,§]**

Nanotechnology Research Institute, National Institute of Advanced Industrial Science and Technology, 1-1-1 Higashi, Tsukuba, Ibaraki 305-8565, Japan, R&D Center, Toda Kogyo Corporation, Otake, Hiroshima 739-0652, Japan, and Faculty of Science, Toho University, 2-2-1 Miyama, Funabashi, Chiba 274-8510, Japan

**ABSTRACT** Energy-filtering electron transmission spectroscopy observation has been achieved to elucidate the nanostructures of powdery nanohybrids, which were produced by the dry mechanical milling of organic pigments and silica nanoparticles. The hybrids possess core−shell structures, irrespective of the levels of aggregation of primary particles, whereas hollow sites of aggregates of primary silica particles were filled with the pigment, leading to the locally concentrated distribution of the pigment to reduce the surface areas of the hybrids. The results imply that nanohybridization is referred to as the buildup method, although mechanical tools and procedures are quite the same as those for the conventional breakdown method.

**KEYWORDS:** core−shell materials • nanoparticles • EFTEM • organic pigment

The dry-milling method is inexpensive and ecologically clean to produce solid particles of desired sizes in large scale and has been extensively employed (1). It should be noticed, however, that the nanodownsizing of organic solids including pigments is problematic without taking into account their characteristics including aggregation, recrystallization, and polymorphism under dry and mechanical conditions (2). Besides, the particle size distribution of milled pigments is wide because of the inherent nature of the top-down process. In a contrast to the conventional milling technique, quite a different approach referred to as the mass-transfer milling to perform the nanodownsizing of organic pigments has recently been reported (3a). The procedure consists of grinding a dry mixture of an organic pigment and silica powders under optimized conditions to result in the formation of nanohybrids (3b), which exhibit no changes in their crystal structure and visible absorption spectra in dispersions (3a) and are applicable to pigmented color filters (3c), inkjet inks (3d), and so forth. The core−shell structuring of the hybrids was inferred by transmission electron microscopy (TEM) observation, which disclosed that the size distribution of primary particles is controllable by weight ratios of a pigment and silica nanopowders and their specific density. In this context, the direct observation of these types of novel organic−inorganic core−shell nanohybrids is highly required in order to elucidate the mechanism of core−shell structuring and to optimize their preparative conditions. Energy-filtering TEM (EFTEM) is a distinctive tool for elemental mapping at high spatial resolution to perform visualization of multicomponent systems in nanoscale. Accordingly, there have been current studies on the visualization of inorganic as well as organic nanoparticles (4), interfaces of binary polymer solids (5), and target compounds in biological cells (6). We report here EFTEM images of the nanohybrid powders consisting of organic pigments and silica nanoparticles to reveal their core−shell structuring. A single silica nanoparticle as a spherical core is, in fact, coated homogeneously with an ultrathin layer of pigment, whereas aggregates of primary silica nanoparticles are also covered with pigment shell layers even though the surface structures of the silica aggregates are complicated.

**Table 1. Nanohybrid Powders of Organic Pigments**

| sample | pigment | pigment:m-$SiO_2$ | $S_{BET}$ ($m^2$/g) |
|---|---|---|---|
| m-$SiO_2$ | non | 0:1 | 154.0 |
| PcB-0.5/1 | PcB[a] | 0.5:1 | 106.8 |
| PcB-1/1 | PcB | 1:1 | 86.6 |
| PcB-2/1 | PcB | 2:1 | 63.9 |
| PcB-3/1 | PcB | 3:1 | 48.4 |
| PcG-1/1 | PcG[b] | 1:1 | 88.7 |
| DKP-1/1 | DKP[c] | 1:1 | 79.4 |

[a] Phthalocyanine blue. [b] Phthalocyanine green. [c] Diketopyrrolopyrrole.

Powders of pigment hybrids and surface-modified silica (m-$SiO_2$) used in this work are listed in Table 1. EFTEM measurements of a powdery nanohybrid of PcB-1/1 prepared by the milling of a 1:1 (w/w) mixture of phthalocyanine blue (PcB) and m-$SiO_2$ were undertaken at room temperature, taking into consideration that PcB exhibits relatively high resistivity against an electron beam (7). Our previous TEM observation showed that primary nanopar-

* To whom correspondence should be addressed. E-mail: k-ichimura@sci.toho-u.ac.jp.

Received for review February 2, 2009 and accepted April 13, 2009

[†] National Institute of Advanced Industrial Science and Technology.

[‡] Toda Kogyo Corp.

[§] Toho University.

DOI: 10.1021/am900066y

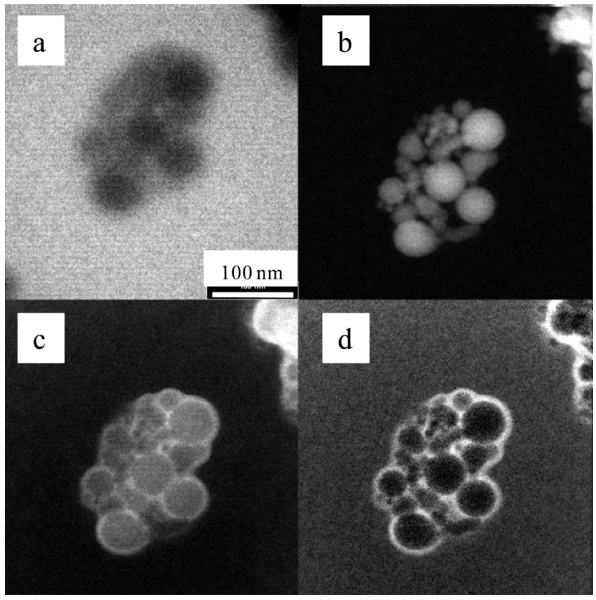


**FIGURE 1. EFTEM images of PcB-1/1 taken at (a) 0 ± 10 eV for the zero-loss image, (b) 262 ± 10 eV for the preedge image, (c) 305 ± 10 eV for the postedge image, and (d) the elemental map of the C atom.**

ticles of PcB-1/1 exhibit multifarious levels of their aggregation including isolated single particles (3). It followed that EFTEM images of an aggregated particle and a single particle of PcB-1/1 were recorded as follows. A plasma-polymerized osmium oxide film (8) was deposited on a cleaved KCl plate by the direct-current glow charge method using a plasma coater (OP80NT, Filgen Inc., Aichi, Japan), followed by dissolution of KCl in water to obtain a thin $OsO_4$ film, which was transferred onto a TEM grid. Nanohybrid powders were kneaded with water to give a paste, which was coated on the non-carbon supporting film and air-dried. EFTEM observation was achieved by using an LEO922 (Carl Zeiss) in-column-type with a $LaB_6$ cathode equipped with an $\omega$-type energy spectrometer at an accelerating voltage of 200 keV at room temperature. Figure 1 shows a series of images for the C elemental mapping by EFTEM for one of the aggregated particles of PcB-1/1. Whereas a zero-loss image (Figure 1a), which was created with elastically scattered electrons, gave no details on core−shell structuring, the preedge image (Figure 1b) and the postedge image (Figure 1c) for the carbon K-shell ionization edge (carbon K-edge) at 285 eV clearly indicated the location of carbon-rich layer on the surface of the individual particles. We can see the drastic change in the contrast by an energy jump beyond the carbon K-edge, showing the presence of the carbon-rich pigment layer outside of the silica particles. Such a distinct contrast difference can be achieved only by using a non-carbon $OsO_4$ supporting film. Figure 1d is a C elemental map calculated by a three-window power law method using two preedge images for the background calculation at 250 ± 10 and 270 ± 10 eV energy losses. The contrast differences among the three images indicate that the particle shown by the preedge image corresponds to the silica particles only, where the aggregate is comprised of many primary particles of silica with a spherical shape and different diameters, while the postedge image shows the entire structure of the hybrid particle, demonstrating evidently that silica particles are covered with PcB layers exhibiting homogeneous thickness. It is worth noting also that PcB penetrates deeply into internal regions of the aggregated particle even though the surface morphology is quite complicated to result in the core−shell nanostructuring, where the aggregates of silica nanoparticles act as cores.

A straightforward core−shell nanostructure was visualized by the C elemental mapping of an isolated particle of PcB-1/1, as shown in Figure 2a. The cross-sectional intensity profile of the carbon distribution image is displayed in Figure 2b and reveals that the intensity curve is almost symmetrical, indicating that the surface of the core silica is sheltered homogeneously with a PcB layer. The particle is entirely spherical in shape with an outside diameter of 58.0 nm, while the diameter is exceptionally larger than the average one of primary particles of 18.2 nm, which was estimated by a TEM image (3a). As described in our previous paper (3a), the shell layer thickness of a hybridized primary particle is determined by a loading weight ratio and a specific density of PcB and silica particles so that the theoretical thickness of a primary particle of PcB-1/1 is calculated to be 2.2 nm. An intensity profile was calculated using a model of a core−shell particle in which a homogeneous carbon-rich layer with a thickness of 4 nm surrounds a silica particle with 50 nm diameter, as shown in Figure 2b, showing a nice agreement with the calculated profile from the achieved carbon distribution image. The results allow us to conclude that the buildup milling gives an indefectible core−shell-type nanostructure. Note here that the silica particles are surface-modified with polysiloxane to improve the affinity of the particle surface to the pigment. Because the loaded amount of silicon resin is 40 mg/g of silica (3a) and quite small when compared with that of 1 g/g of silica of PcB, the contribution of C atoms of the surface modifier to the C mapping is negligibly small. It should be mentioned that particles solely visualized with Si-mapped or C-mapped images are not observed at all not only in Figures 1 and 2 but also in EFTEM images of the other particles, supporting the thorough nanohybridization.

The other PcB hybrids were subjected to EFTEM analysis to disclose the influence of the loading ratio of the pigment on the core−shell nanostructures. It was confirmed again that the surface of aggregated silica particles of PcB-0.5/1 is evenly layered by a PcB shell, as shown in Figure S1 in the Supporting Information (9). On the other hand, irregular C maps are viewed when loading ratios of PcB are increased. As shown in Figure S2a in the Supporting Information, the carbon distribution image of an aggregated particle of PcB-2/1 presented uniform thickness in a manner quite similar to those of PcB-0.5/1 and PcB-1/1, revealing that the aggregated silica core is homogeneously covered with a PcB shell layer. On the other hand, locally brighter areas are observed in the carbon distribution images of the other nanohybridized aggregates, as seen in Figure S2b in the Supporting Information (9). This situation indicates the local

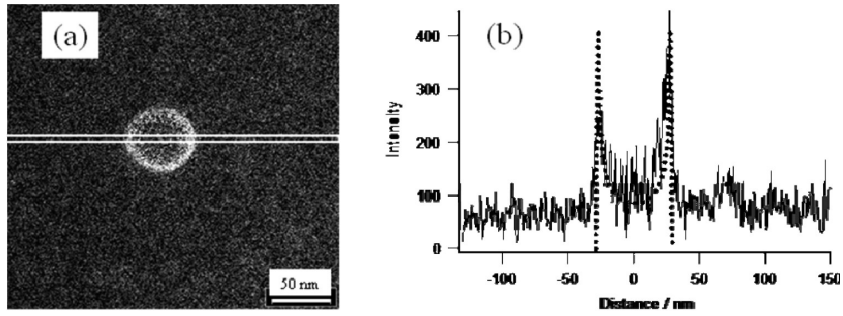


FIGURE 2. (a) C map of a single nanohybrid particle of PcB-1/1 and (b) cross-sectional intensity of the C map as a function of the distance (solid line) and a theoretical curve for the C intensity of the particle, assuming that the outside diameter and thickness of a PcB shell are 58.0 and 2.2 nm, respectively.

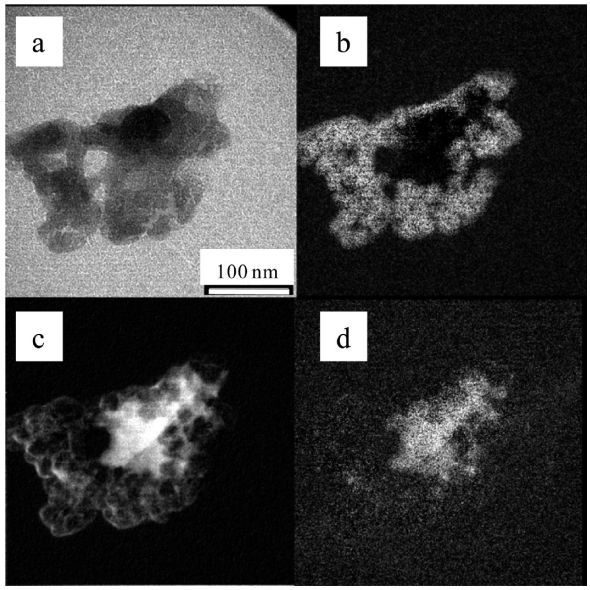


FIGURE 3. EFTEM images of PcB-3/1: (a) zero loss; (b) Si map; (c) C map; (d) N map.

condensation of PcB, implying that the pigment is filled in hollow spaces of the silica aggregates. Because quite similar results were obtained for PcB-3/1, a more detailed analysis was performed, as displayed in Figure 3. The aggregated particle exhibits a very complicated structure, as shown in a zero-loss image (Figure 3a), and the uneven distribution of the pigment on the aggregated silica particles is clearly visualized by the silicon, carbon, and nitrogen distribution images. Whereas the carbon and nitrogen distribution images exhibit the same trends in terms of the location and concentration of the elements, the bright regions in the carbon and nitrogen distribution images approximately correspond to the dark regions in the silicon distribution image. This situation discloses that perplexingly complicated spaces of the silica aggregates are filled with the pigment, whereas the whole surface areas are covered with a pigment layer of relatively even thickness. It is notable that a clear-cut core–shell nanostructure is observable for PcB-3/1 even though the loading weight of the pigment is 3 times larger than that of core silica. Figure 4 shows silicon and carbon distribution images of a twin particle of PcB-3/1 as examples. The diameters of the smaller particles of the twin estimated from the silicon and carbon distribution images are ca. 36 and 45 nm, respectively, so that a shell thickness can be

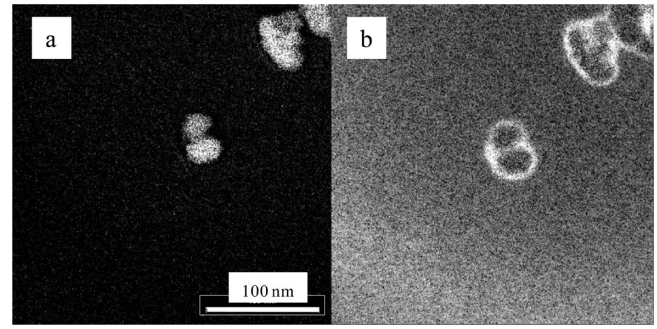


FIGURE 4. EFTEM images of particles of PcB-3/1: (a) Si map; (b) C map.

estimated to be 4.5 nm and somewhat thinner than the theoretical one of 4.8 nm. This result stems probably from the local filling of the pigment at the joint part of the twin.

The mass-transfer milling has been reported to be applicable to various kinds of organic pigments so that EFTEM analysis was performed for the 1:1 (w/w) hybrids of phthalocyanine green (PcG) and diketopyrrolopyrrole (DKP) red pigments. Figure 5 shows typical results of C and Si mapping for PcG-1/1. In analogy to PcB-1/1, the surface of aggregated silica nanoparticles is homogeneously coated with a PcG layer, as shown in Figure 5a. Figure 5b displays the carbon distribution image of another aggregated particle of PcG-1/1, suggesting the existence of local carbon-concentrated regions. Note here that an isolated particle containing no silicon was detected, as highlighted by the circles, indicating the presence of the nonhybridized PcG particles. Such nonhybridized particles of silica or the pigments could not be detected in all of the other samples so it is safe to draw the conclusion that the milling of a mixture of PcG and silica nanoparticles gives rise to sufficient hybridization. It has been generally known that cryoobservation is effective for reducing the damage of the specimen, which sometimes causes structural changes of a specimen (10). We have confirmed that cryoobservation gives the same results, as shown in Figure 3S in the Supporting Information (9). A core–shell structure was observed in a carbon distribution image, confirming that PcG shows no signs of the significant structural changes by electron-beam bombardment at room temperature. Furthermore, when cooling, the analysis suffered from heavy drift and contamination of the specimen. Thus, no advantages were found in the time-consuming cryoobservation in this study.

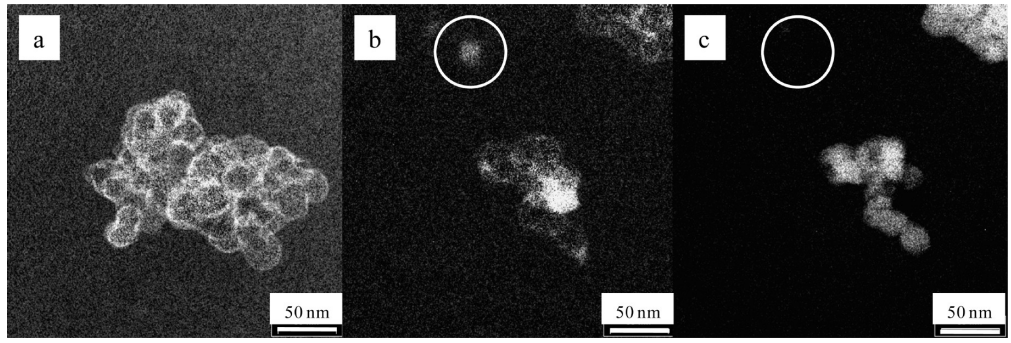


**FIGURE 5. (a) C map of a hybridized aggregate of PcG-1/1. (b) C map and (c) Si map of the other aggregates. The circles indicate the particle consisting solely of PcG.**

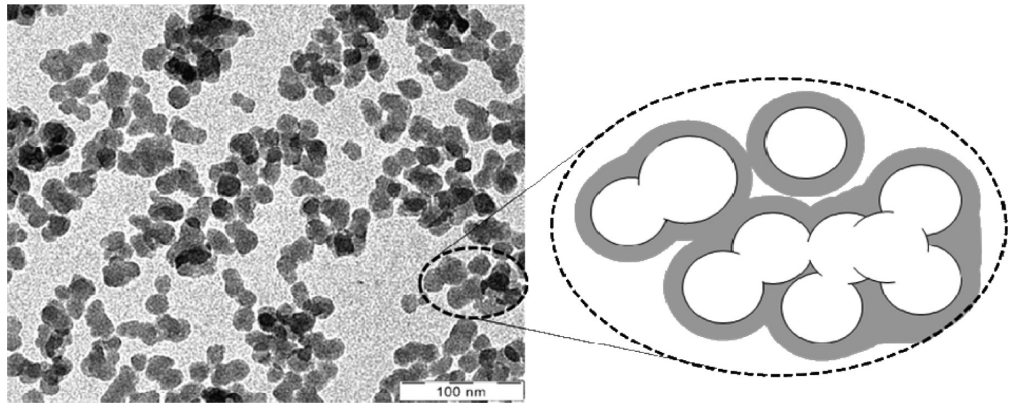


**FIGURE 6. TEM image and illustrative presentation of core–shell structures of PcB-1/1 particles.**

DKP displayed a hybridization behavior somewhat different from that of PcB and PcG, as shown in Figure S4 in the Supporting Information (9). In contrast to the cases of PcB and PcG shown in Figures 1d and 5a, respectively, an aggregated hybrid particle displayed the local condensation of the pigment as visualized by bright areas, even though the mixing ratio is 1:1 in weight, suggesting that DKP forms an ultrathin shell layer on silica nanoparticles more reluctantly when compared with PcB and PcG. This is probably because of the inherent nature of DKP molecules in solids. Whereas intermolecular forces stemming from van der Waals and $\pi-\pi$ interactions play major roles in both phthalocyanine pigments, intermolecular double-bridged hydrogen bonds causing high polarity play an additional role in the DKP pigment so that the cohesive interactions of DKP molecules or clusters with a hydrophobic surface of silica nanoparticles are reduced when compared with the phthalocyanine pigments.

Brunauer–Emmett–Teller (BET) specific surface areas ($S_{BET}$) summarized in Table 1 give valuable information concerning the surface morphology of nanohybrids. The m-$SiO_2$ nanoparticles used for the preparation of the pigment hybrids possess a $S_{BET}$ value of 154 $m^2/g$ of silica, and the $S_{BET}$ values of a family of PcB hybrids decrease with the increment of the loading weight ratios of PcB. In particular, $S_{BET}$ of PcB-3/1 is only about one-third of that of m-$SiO_2$. The marked reduction of $S_{BET}$ arises unequivocally from the fact that hollow spaces formed by the fusion of primary silica nanoparticles are filled with PcB in such a way that the intricate surface becomes much smoother, as discussed above, leading to the reduction of surface areas. Whereas $S_{BET}$ values of PcB-1/1 and PcG-1/1 are not far from each other, DKP-1/1 exhibits a slightly smaller value when compared with those of the hybrids of the phthalocyanine pigments. Such a difference arises from the inherent nature of the red pigment to incline to locally concentrated cohesion on hydrophobic particle surfaces, as discussed above.

The visualization of the core–shell nanostructure shown above is of crucial importance to distinguishing the mass-transfer milling from the conventional breakdown milling. As suggested in our previous paper (3a), the essence of the milling in the presence of silica nanoparticles exists not in the mechanical crash of a pigment solid termed as a conventional breakdown process but in the cumulative cohesion of the pigment on surfaces of silica primary particles during the dry milling. We attract attention accordingly to the fact that the present milling technique belongs to a novel buildup process even though tools and procedures for the established milling are utilizable. This situation is of practical significance because of the large-scale productivity of pigment nanohybrids. In this context, the elucidation of the buildup mechanism is very curious and important. One of the clues to revealing the mechanism is the necessity of the modification of silica nanoparticles with a polysiloxane. As mentioned in our previous paper (3a), hybridization does not occur at all when silica powders with a bare surface with high polarity are used. Consequently, it is assumed that the affinity of a pigment to silica nanoparticles is dramatically improved by surface modification. The next question is why a pigment as a solid material is deposited on the nanoparticle surfaces

uniformly solely by the mechanical treatment in the solid state. We have reported recently that the dry milling of a mixture of crystal violet lactone (CVL) crystals and silica nanoparticles results in Langmuir-type adsorption through hydrogen bonds to form a monolayer of the cationic ring-opened triphenylmethane dye derived from CVL (11). Besides, the solid-state Langmuir isotherms under dry-milling conditions were also observed for adsorption of oligo(ethylene glycol) and nonionic surfactants onto a bare surface of silica nanoparticles. In this respect, a pigment is likely adsorbed on hydrophobic surfaces of silica nanoparticles through van der Waals interactions. On the other hand, it is hard to anticipate that adsorption occurs in a molecule-to-molecule fashion because interactions among pigment molecules are quite strong and no changes in the crystal structures were observed (3a). It is reasonably assumed that a pigment is ground to give nanosized solid fragments, which are, in turn, adsorbed on silica nanoparticles, because no modification of the crystal structure of PcB was observed (3a). The nanodownsizing of the pigment is accelerated by silica nanoparticles so that silica nanoparticles may play dual roles as nanoballs to perform nanomilling of the pigment and as cores to be deposited by a nanofragmented pigment to lead to core−shell nanostructuring.

In conclusion, EFTEM observation revealed unequivocally that the hybrid powders fabricated by the dry milling of organic pigments and m-$SiO_2$ possess core−shell structures, irrespective of the levels of aggregation of primary particles. A shell layer thickness of a 1:1 hybrid of PcB and m-$SiO_2$ is in good agreement with the theoretical one determined by the mixing weight ratio and specific density of both components. Hollow sites of aggregates of primary silica particles are filled with a pigment, leading to the locally concentrated distribution of the pigment to reduce the surface areas of the hybrid. The results allow us to draw an illustrative presentation of the hybrid, as shown in Figure 6. The other pigment hybrids possess similar core−shell structures. It was assumed that m-$SiO_2$ may play a dual role, acting as nanosized balls to grind pigment particles and as cores, on which pigment nanofragments thus formed are cohered as a result of hydrophobic interactions between a silica surface and the pigment. Accordingly, nanohybridization is referred to as the buildup method for the preparation of nanoparticles, although mechanical tools and procedures are quite the same as those employed for the conventional breakdown method.

**Acknowledgment.** The authors are indebted to Toda Kogyo Corp., Ltd., for the gift of the pigment hybrids and to Dr. K. Yase of the National Institute of Advanced Industrial Science and Technology for his discussion and encouragement throughout this work.

**Supporting Information Available:** Additional TEM images and element maps (Figures S1−S4). This material is available free of charge via the Internet at http://pubs.acs.org.

## REFERENCES AND NOTES

(1) Karagedov, G. R.; Lyakhov, N. Z. *KONA* **2003**, *21*, 76–86.
(2) Boldyrev, V. V. *J. Mater. Sci.* **2004**, *39*, 5117–5120.
(3) (a) Hayashi, K.; Morii, H.; Iwasaki, K.; Horie, S.; Horiishi, N.; Ichimura, K. *J. Mater. Chem.* **2007**, *17*, 527–530. (b) Hayashi, K.; Ohsugi, M.; Iwasaki, K.; Morii, H. (Toda Kogyo Corp.) U.S. Patent 7,022,752, 2006. (c) Ichimura, K.; Hayashi, K.; Morii, H. (Toda Kogyo Corp.) U.S. Patent 7,157,025, 2007. (d) Hayashi, K.; Morii, H.; Iwasaki, K. (Toda Kogyo Corp.) U.S. Patent 6,623,557, 2003.
(4) (a) Horiuchi, S.; Dohi, H. *Langmuir* **2006**, *22*, 4607–4613. (b) Trabelsi, S.; Fornasieri, G.; Rozes, L.; Janke, A.; Mensch, A.; Sanchez, C.; Stamm, M. *J. Appl. Crystallogr.* **2006**, *39*, 656–660. (c) Dohi, H.; Horiuchi, S. *Langmuir* **2007**, *23*, 12344–12349. (d) Valadares, L. F.; Bragança, F. do C.; da Silva, C. A.; Leite, C. A. P.; Galembeck, F. *J. Colloid Interface Sci.* **2007**, *309*, 140–148. (e) Linares, E. M.; Leite, C. A. P.; Valadares, L. F.; Silva, C. A.; Rezende, C. A.; Galembeck, F. *Anal. Chem.* **2009**, *81*, 2317–2324.
(5) (a) Horiuchi, S.; Yin, D.; Ougizawa, T. *Macromol. Chem. Phys.* **2005**, *206*, 725–731. (b) Hayakawa, T.; Goseki, R.; Kakimoto, M.; Tokita, M.; Watanabe, J.; Liao, Y.; Horiuchi, S. *Org. Lett.* **2006**, 5453–5456. (c) Liao, Y.; Horiuchi, S.; Nunoshige, J.; Akahoshi, H.; Ueda, M. *Polymer* **2007**, *48*, 3749–3758.
(6) (a) Koop, A.; Voss, I.; Thesing, A.; Kohl, H.; Reichelt, R.; Steinbüchel, A. *Environ. Sci. Technol.* **2007**, *41*, 3012–3017. (b) Koop, A.; Voss, I.; Thesing, A.; Kohl, H.; Reichelt, R.; Steinbüchel, A. *Biomacromolecules* **2007**, *8*, 2675–2683. (c) Lütz-Meindl, U. *Micron* **2007**, *38*, 181–196.
(7) (a) Reimer, L. *Transmission Electron Microscopy*; Springer-Verlag: Berlin, 1997; pp 463−494. (b) Hayashida, M.; Kawasaki, T.; Kimura, Y.; Takai, Y. *Nucl. Instrum. Methods Phys. Res., Sect. B* **2006**, *248*, 273–278.
(8) Tanaka, A. *J. Electron Microsc.* **1994**, *43*, 177–182.
(9) See the Supporting Information.
(10) Li, P.; Egerton, R. F. *Ultramicroscopy* **2004**, *101*, 161–172.
(11) Ichimura, K.; Funabiki, A.; Aoki, K.; Akiyama, H. *Langmuir* **2008**, *24*, 6470–6479.

AM900066Y